Research Article

NEURAL REGENERATION RESEARCH
www.nrronline.org

Ruxolitinib attenuates secondary injury after traumatic spinal cord injury

https://doi.org/10.4103/1673-5374.335165

Date of submission: July 26, 2021

Date of decision: October 27, 2021

Date of acceptance: November 29, 2021

Date of web publication: February 8, 2022

Zhan-Yang Qian[1, 2, #], Ren-Yi Kong[3, #], Sheng Zhang[3, #], Bin-Yu Wang[3], Jie Chang[3], Jiang Cao[3], Chao-Qin Wu[3], Zi-Yan Huang[3], Ao Duan[3], Hai-Jun Li[4, 5, *], Lei Yang[4, 5, *], Xiao-Jian Cao[3, *]

From the Contents

Graphical Abstract *Mechanism of ruxolitinib activity against inflammatory pathology post-spinal cord injury*

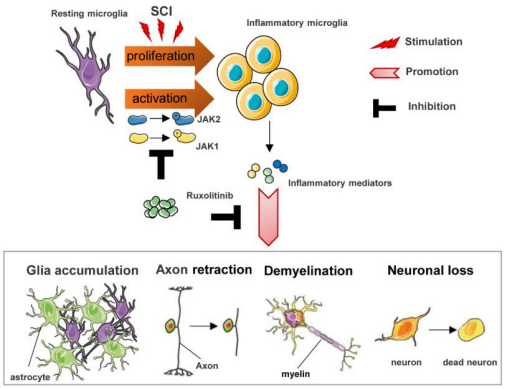

Abstract

Excessive inflammation post-traumatic spinal cord injury (SCI) induces microglial activation, which leads to prolonged neurological dysfunction. However, the mechanism underlying microglial activation-induced neuroinflammation remains poorly understood. Ruxolitinib (RUX), a selective inhibitor of JAK1/2, was recently reported to inhibit inflammatory storms caused by SARS-CoV-2 in the lung. However, its role in disrupting inflammation post-SCI has not been confirmed. In this study, microglia were treated with RUX for 24 hours and then activated with interferon-γ for 6 hours. The results showed that interferon-γ-induced phosphorylation of JAK and STAT in microglia was inhibited, and the mRNA expression levels of pro-inflammatory cytokines tumor necrosis factor-α, interleukin-1β, interleukin-6, and cell proliferation marker Ki67 were reduced. In further *in vivo* experiments, a mouse model of spinal cord injury was treated intragastrically with RUX for 3 successive days, and the findings suggest that RUX can inhibit microglial proliferation by inhibiting the interferon-γ/JAK/STAT pathway. Moreover, microglia treated with RUX centripetally migrated toward injured foci, remaining limited and compacted within the glial scar, which resulted in axon preservation and less demyelination. Moreover, the protein expression levels of tumor necrosis factor-α, interleukin-1β, and interleukin-6 were reduced. The neuromotor function of SCI mice also recovered. These findings suggest that RUX can inhibit neuroinflammation through inhibiting the interferon-γ/JAK/STAT pathway, thereby reducing secondary injury after SCI and producing neuroprotective effects.

Key Words: functional recovery; glial scar; inflammation; interferon-γ; JAK/STAT signaling; microglia; Ruxolitinib; spinal cord injury

Introduction

Trauma causes acute mechanical spinal cord injury (SCI), which further elicits prominent pathological events post-SCI (Ahuja et al., 2017; Ren et al., 2018). The neuronal death, myelin destruction, and vascular disruption that occur after SCI promote inflammation and initiate a sequence of secondary neuropathological events, including scar formation, which impedes axonal regeneration and functional recovery (Silva et al., 2014; Zhou et al., 2019). Microglia, which are the resident immune cells in neurological tissue (Madore et al., 2020), respond to injury immediately after SCI and contribute to activation of neuroinflammation (David and Kroner, 2011; Saijo and Glass, 2011; Kroner and Rosas Almanza, 2019). Indeed, activated microglia secrete inflammatory cytokines that degrade enzymes, leading to the generation of myelin debris and the assembly of the glial scar, which not only promote inflammation but also cause axonal regeneration failure and axonal dysfunction (Aguzzi et al., 2013; Kroner and Rosas Almanza, 2019). Therefore, suppression of microglial activation is crucial for neuronal survival, myelin preservation, and resolution of inflammation.

[1]Spine Center, Zhongda Hospital of Southeast University, Nanjing, Jiangsu Province, China; [2]Medical School, Southeast University, Nanjing, Jiangsu Province, China; [3]Department of Orthopedics, First Affiliated Hospital of Nanjing Medical University, Nanjing, Jiangsu Province, China; [4]Department of Orthopedics, Hospital Affiliated 5 to Nantong University (Taizhou People's Hospital), Taizhou, Jiangsu Province, China; [5]Taizhou Clinical Medical School of Nanjing Medical University, Taizhou People's Hospital, Taizhou, Jiangsu Province, China

*Correspondence to: Xiao-Jian Cao, MD, PhD, xiaojiancao001@163.com; Lei Yang, PhD, leiyang@njmu.edu.cn; Hai-Jun Li, MD, PhD, 13901436563@139.com.
https://orcid.org/0000-0001-5567-0536 (Xiao-Jian Cao); https://orcid.org/0000-0001-5677-9955 (Lei Yang)
#These authors contributed equally to this work.

Funding: *The study was supported by the National Natural Science Foundation of China, Nos. 81871773 (to XJC), 81672152 (to XJC), 81802149 (to LY); Primary Research and Development Plan of Jiangsu Province of China, No. BE2018132 (to XJC); and Scientific Research Project of Health Commission of Jiangsu Province of China, No. LGY2020068 (to HJL).*

How to cite this article: *Qian ZY, Kong RY, Zhang S, Wang BY, Chang J, Cao J, Wu CQ, Huang ZY, Duan A, Li HJ, Yang L, Cao XJ (2022) Ruxolitinib attenuates secondary injury after traumatic spinal cord injury. Neural Regen Res 17(9):2029-2035.*

Interferon-γ (IFN-γ), a biomarker of Th1 cells, is a pro-inflammatory cytokine that stimulates various immune effector cells, including macrophages, nature killer cells, cytotoxic T cells, and microglia, to activate inflammation (Kelchtermans et al., 2008; Too and Mitchell, 2021). During neuropathological events, IFN-γ enables brain dendritic cells to transform into effective antigen-presenting cells and exacerbates oligodendrocyte apoptosis, which leads to demyelination and enhanced microglia-induced neuronal dysfunction and death (Pouly et al., 2000; Gottfried-Blackmore et al., 2009; Papageorgiou et al., 2016). IFN-γ activation is dependent on activation of the Janus kinase (JAK)-signal transducer and activator of transcription (STAT) axis, which is a known inflammation-related signaling pathway (Delen and Doğanlar, 2020). Ruxolitinib (RUX), a selective JAK1 and JAK2 inhibitor, was approved for treatment of myelofibrosis by the U.S. Food and Drug Administration in 2011 and the European Medicines Agency in 2012 (Ajayi et al., 2018). Recent studies have shown that RUX is a strong inhibitor of the "cytokine storm" that occurs in patients with coronavirus disease 2019 (Cao et al., 2020; Huarte et al., 2021; Yan et al., 2021). Moreover, RUX has been demonstrated to reduce inflammation in innate immune colitis and lipopolysaccharide-induced ocular inflammation (Overstreet et al., 2018; Liang et al., 2020). Collectively, these above-mentioned studies have indicated that there is a link between RUX-mediated inhibition of inflammation and the IFN-γ/JAK/STAT signaling pathway in microglia; however, whether RUX can reduce inflammation after SCI remains to be elucidated.

In the present study, we hypothesized a previously unreported role for RUX-mediated inhibition of the post-SCI microglial-induced neuroinflammatory response. We investigated the effects of RUX on the pro-inflammatory cascades and microglial proliferation regulated by the IFN-γ/JAK1-2/STAT1 axis in an *in vitro* model of IFN-γ-induced microglial inflammation and clarified the pharmacological effects of RUX on inflammation-induced neuropathology, including myelinoclasis, neuronal loss, and glial scar formation, in a mouse model of SCI.

Materials and Methods

Cell lines and culture conditions

The microglia cell line BV2 (Cat# 0356; RRID: CVCL_0182), which has been short tandem repeat genotyped, was purchased from the Institute of Cell Research, Chinese Academy of Medical Sciences (Shanghai, China). Cells were cultured in Dulbecco's modified Eagle medium (Cat# G4510; Servicebio, Wuhan, China) with 10% fetal bovine serum (Invitrogen, Carlsbad, CA, USA) and 1% penicillin-streptomycin (Servicebio), as previously described (Hong et al., 2020). RUX (Cat# ab141356; Abcam, Cambridge, MA, USA) was dissolved in pH 3.5 citrate buffer according to a previous study (Das et al., 2016). Microglia were pretreated with 0.1, 0.5, or 1 mM RUX for 24 hours, followed by treatment with IFN-γ (20 ng/mL; Invitrogen) for 6 hours.

Animals

Human SCI prevalence is higher in men (~80%) than in women, according to the 2019 SCI Data Sheet from the National SCI Statistical Center (Li et al., 2020). Thus, a total of 30 male adult C57BL/6J mice (8 weeks old, 18–20 g) were purchased from the Experimental Animal Center of Nanjing Medical University (license No. SYXK2021-0023) and housed in a specific pathogen-free environment. This study was approved by the Institutional Animal Care and Use Committee of Southeast University (approval No.20210302042; March 2, 2021). All experiments were designed and reported according to the Animal Research: Reporting of *In Vivo* Experiments (ARRIVE) guidelines (Percie du Sert et al., 2020).

Mice were randomly divided into three groups (n = 6): (i) Sham group: mice underwent laminectomy; (ii) SCI group: mice with SCI and daily intragastric administration of an oral dose of citrate buffer (0.1 mL) equivalent to the RUX dose; and (iii) SCI + RUX group: mice with SCI and intragastric administration of RUX at 50 mg/kg per day. RUX was initially administered 2 hours after SCI and continued for 3 days. The protocol for the SCI model was described in our previous report (Hong et al., 2020). Briefly, mice were anesthetized with ketamine (80 mg/kg; Hengrui Pharma, Lianyungang, China) and xylazine (4 mg/kg; MilliporeSigma, Burligton, MA, USA), after which a laminectomy was performed. A 5-g spinal cord impactor (68097, RWD, Shenzhen, China) at a height of 5 cm was used to create a SCI at T10.

Cell viability assay

Microglia (1×10^4/well) were seeded in a 96-well plate and then with a concentration gradient of RUX (0.1–5 mM) for 24 hours. Then, the cells were washed twice and incubated with 100 μL Dulbecco's modified Eagle medium containing 10% cell counting kit-8 (Cat# C0038; Beyotime, Shanghai, China) buffer for 2 hours at 37°C. Detection was carried out at 450 nm using a microplate reader (BioTek, Friedrichshall, Germany), and analysis was performed using ImageJ software (Ver. 1.3.8) (Schneider et al., 2012).

Quantitative polymerase chain reaction

To perform a preliminary investigation of the effect of RUX on microglial inflammation, RNA was extracted from microglia using Trizol (Yifeixue Biotech, Nanjing, China). The isolated RNA was reverse transcribed using a GoldenstarTM RT6 cDNA Synthesis Kit (TsingKe, Beijing, China), after which a quantitative polymerase chain reaction was performed to quantify the levels of target genes using SYBR Green Master (TsingKe). Briefly, RNA was denatured at 95°C for 2 minutes, then a total of 35 cycles were carried out, each of which included denaturation at 95°C for 15 seconds, annealing at 60°C for 15 seconds, and extension at 72°C for 30 seconds. The primer sequences are listed in **Table 1**. Expression levels were normalized to GADPH using the $2^{-\Delta\Delta Ct}$ method (Livak and Schmittgen, 2001).

Table 1 | **Primers used for quantitative polymerase chain reaction**

Gene	Sequence (5'–3')
TNF-α	Forward: CAG GCG GTG CCT ATG TCT C
	Reverse: CGA TCA CCC CGA AGT TCA GTA G
IL-1β	Forward: GCA ACT GTT CCT GAA CTC AAC T
	Reverse: ATC TTT TGG GGT CCG TCA ACT
IL-6	Forward: CTG CAA GAG ACT TCC ATC CAG
	Reverse: AGT GGT ATA GAC AGG TCT GTT GG
IL-10	Forward: CTT ACT GAC TGG CAT GAG GAT CA
	Reverse: GCA GCT CTA GGA GCA TGT GG
IL-27	Forward: ATC TTC CCA ATG TTT CCC TGA C
	Reverse: CCG AAG TGT GGT AGC GAG G
GAPDH	Forward: AGG TCG GTG TGA ACG GAT TTG
	Reverse: TGT AGA CCA TGT AGT TGA GGT CA

GAPDH: Glyceraldehyde-3-phosphate dehydrogenase; IL-10: interleukin-10; IL-1β: interleukin-1β; IL-27: interleukin-27; IL-6: interleukin-6; TNF-α: tumor necrosis factor-α.

Western blot assay

To detect the expression of inflammation-related signaling and mediators, protein was extracted from microglia using a total protein extraction kit (KeyGEN, Nanjing, China) after treatment with IFN-γ for 6 hours. After quantification using the bicinchoninic acid method (Walker, 1994), an equal amount of protein from each group was subjected to sodium dodecyl sulfate polyacrylamide gel electrophoresis and transferred to a polyvinylidene fluoride membrane (Millipore, Billerica, MA, USA), which was then blocked in 5% skim milk for 1 hour at room temperature and incubated with primary antibodies overnight at 4°C and secondary antibodies for 1 hour at room temperature. The antibodies used were as follows: rabbit anti-phosphorylated (p)-Janus kinase (JAK) 1 (Cat# 74129; RRID:AB_2799851; 1:1000; Cell Signaling Technology, Danvers, MA, USA), rabbit anti-JAK1 (Cat# 3344; RRID:AB_2265054; 1:1000; Cell Signaling Technology), rabbit anti-p-JAK2 (Cat# 3771; RRID:AB_330403; 1:1000; Cell Signaling Technology), rabbit anti-JAK2 (Cat# 3230; RRID:AB_2128522; 1:1000; Cell Signaling Technology), rabbit anti-p-STAT1 (Cat# 9167; RRID:AB_561284; 1:1000; Cell Signaling Technology), rabbit anti-STAT1 (Cat# 14994; RRID:AB_2737027; 1:1000; Cell Signaling Technology), rabbit anti–inducible nitric oxide synthase (iNOS; Cat# ab15323; RRID:AB_301857; 1:250; Abcam), rabbit anti-cyclooxygenase (COX)-2 (Cat# ab179800; 1:1000; Abcam), mouse anti-glyceraldehyde-3-phosphate dehydrogenase (Cat# HRP-60004; RRID:AB_2737588; 1:10,000; Proteintech, Chicago, IL, USA), and horse radish peroxidase goat anti-rabbit or -mouse conjugated secondary antibodies (Cat# YFSA01; Cat# YFSA02; 1:10,000; Yifeixue Biotech). An enhanced chemiluminescence system (Tanon, Shanghai, China) was employed to examine the levels of protein, and ImageJ software (Schneider et al., 2012) was used for quantification.

Enzyme-linked immunosorbent assay

To measure cytokine levels, mice were sacrificed with excess ketamine/xylazine, and 2 cm of spinal cord tissue from the center of the lesion (weighing 0.03 g) was removed, homogenized, and centrifuged at 4°C. The samples were then stored at −80°C until further use. Inflammatory markers (tumor necrosis factor (TNF)-α, interleukin (IL)-1β, IL-6, IL-10, and IL-27) were measured using the respective enzyme-linked immunosorbent assay kits (Invitrogen), following the manufacturer's protocols. Absorbance was detected at 550 nm using a microplate reader.

5-Ethynyl-2'-deoxyuridine assay

To determine the proliferative potential, microglia (1×10^5) were added to a 96-well plate and treated with RUX for 24 hours. Next, the cells were incubated with kFluor555-5-ethynyl-2′-deoxyuridine working buffer according to the manufacturer's protocol (Cat# KGA337; KeyGen). The cells were then washed, fixed with 4% paraformaldehyde (PFA; Cat# G1101; Servicebio) for 15 minutes, washed again in 3% bovine serum albumin (Invitrogen), incubated with 0.5% Triton X-100 for 20 minutes, and probed with Click-iT mix in the dark for 30 minutes. Finally, the cells were stained with Hoechst 33342 (MedChemExpress, Shanghai, China) for 30 minutes, and the fluorescence was detected at 555 nm using a fluorescence microscope (Leica, Wetzlar, Germany).

Immunofluorescence staining

Immunofluorescence staining was used to detect the expression of inflammatory mediators *in vitro* and injured cord tissue *in vivo*. Mice at 3, 7, and 28 days post-SCI were anesthetized with ketamine/xylazine, after which the heart was perfused using normal saline and 4% PFA. Spinal cord tissues were then placed in 4% PFA for 2 days, dehydrated using an ethanol gradient, cleared with dimethylbenzene, embedded in paraffin, and sliced into 5-μm sections using a rotary microtome (Leica). Sections were then fixed in 4% PFA for 10 minutes at room temperature, immuno-blocked with a blocking reagent, incubated with primary antibodies overnight at 4°C, and incubated with Alexa Fluor secondary antibodies for 1 hour at room temperature. The antibodies used included: rabbit-anti-p-STAT1 (Cat# 9167; RRID:AB_561284; 1:400; Cell Signaling Technology), mouse anti-glial fibrillary acidic protein (Cat# 3670, RRID: AB_561049, 1:600, Cell Signaling Technology), rabbit anti-ionized calcium-binding adaptor (IBA)1 (1:500, Cat# ab178847, RRID: AB_2832244, Abcam), rabbit anti-iNOS (1:100, Cat# ab15323, RRID: AB_301857, Abcam), rabbit anti-neurofilament heavy polypeptide (1:200, Cat# ab207176, RRID: AB_2827968, Abcam), rabbit anti-Ki67 (1:500, Cat# ab15580, RRID: AB_443209, Abcam), rabbit anti-COX-2 (1:200, Cat# ab179800, Abcam), rabbit anti-TNF-α (1:200, Cat# GB11188, Servicebio), rabbit anti-IL-1β (1:500, Cat# GB11113, Servicebio), rabbit anti-IL-6 (1:500, Cat# GB11117, Servicebio), and Alexa Fluor 488-, 555-, and 647-conjugated secondary antibodies (1:500, Cat# 111587003, RRID: AB_2338071, goat anti-rabbit; Cat# 111547003, RRID: AB_2338058, goat anti-rabbit; Cat# 111607003, RRID: AB_2338084, goat anti-rabbit; Cat# 115586003, RRID: AB_2338890, goat anti-mouse; Jackson ImmunoResearch Labs, Philadelphia, PA, USA). Finally, the sections were counterstained with diamidinyl phenyl indole reagent (Servicebio) and mounted with fluorescence quenching–resistant reagent (G1401; Servicebio). Images were collected using a fluorescence microscope and analyzed using ImageJ software (Schneider et al., 2012).

Histological staining

To visualize histological destruction within the injured spinal cord, 1-cm cord sections from the center of the lesion were stained with hematoxylin-eosin (H&E) at 3, 7, and 28 days post-SCI and Nissl at 7 and 28 days post-SCI in accordance with the respective manufacturers' instructions (Cat# G1036 for Nissl, Cat# G1005 for H&E; Servicebio). For H&E staining, sections were stained with hematoxylin dye for 5 minutes, and then were incubated with eosin dye for 5 minutes. For Nissl staining, sections were placed in Nissl dye for 3 minutes. After mounting with neutral balsam, sections were observed using an optical microscope (Leica). The number of neurons and the tissue integrity were analyzed using ImageJ software (Schneider et al., 2012).

Behavioral tests

Hindlimb movement of SCI mice at 1, 3, 7, 14, and 28 days post-SCI was assessed by the Basso mouse scale and Louisville Swim Scale (LSS). The procedures related to the Basso mouse scale and the LSS have been previously described (Kong et al., 2020). The Basso mouse scale ranges from 0 (no ankle movement) to 9 (complete motor function) points and rates motion according to joint movement, trunk stability, gait coordination, paw placement, and tail position. The 15 points possible on the LSS evaluate forelimb dependency and hindlimb movement and frequency, as well as the angle between the trunk and the water surface. A high score indicates good functional recovery, and a low score indicates poor recovery.

Statistical analysis

No statistical methods were used to predetermine sample sizes; however, our sample sizes are similar to those reported in a previous publication (Huo et al., 2021). No animals or data points were excluded from the analysis. The assessors were blinded to the animal groups. Data are presented as mean ± standard deviation (SD). One-way or two-way analysis of variance followed by Tukey's *post hoc* test was employed to evaluate differences among more than two groups, and unpaired two-tailed Student's *t*-test was used to assess differences between two groups. Data were visualized using GraphPad Prism 8.0 software (GraphPad Software Inc., San Diego, CA, USA). *P*-values < 0.05 were considered statistically significant.

Results

Ruxolitinib inhibits IFN-γ-induced pro-inflammatory effects by targeting the JAK/STAT1 axis

The viability of microglia treated with different doses of RUX was determined by cell counting kit-8 assay at 24 hours post-SCI. The results indicated that concentrations ranging from 0.1 to 1 mM seldom decreased cell viability, while doses at 2 and 5 mM significantly reduced microglial viability (**Figure 1A**). Next, we determined the effect of RUX at 0.1 to 1 mM on microglia pretreated with IFN-γ for 6 hours. The western blot results indicated that the p-JAK1/JAK1 ($P < 0.0001$), p-JAK2/JAK2 ($P = 0.0003$), and p-STAT1/STAT1 ($P < 0.0001$) ratios were significantly reduced after treatment with 1 mM RUX compared with the IFN-γ group (**Figure 1B–E**). We also measured the levels of the pro-inflammatory cytokines TNF-α, IL-1β, and IL-6 and the anti-inflammatory cytokines IL-10 and IL-27. TNF-α ($P < 0.0001$), IL-1β ($P < 0.0001$), and IL-6 ($P < 0.0001$) mRNA levels were markedly decreased in an RUX concentration–dependent manner (**Figure 1F–H**); however, IL-10 ($P = 0.5665$) and IL-27 ($P = 0.0574$) mRNA levels showed no significant changes compared with the IFN-γ group (**Figure 1I** and **J**). Taken together, these data suggest that RUX mitigates IFN-γ-induced pro-inflammatory effects by inhibiting the JAK/STAT1 axis in microglia.

RUX reduces microglial activation and proliferation

To further ascertain the anti-inflammatory role of RUX in IFN-γ-stimulated microglia, we selected 1 mM RUX to examine its effect on polarization. Specifically, the inflammatory marker iNOS was detected in microglia by immunofluorescence, and the results indicated that IFN-γ increased iNOS expression in microglia, but that subsequent treatment with RUX decreased the IFN-γ-stimulated high expression level of iNOS (**Figure 2A**). IL-1β and IL-6 production also increased after IFN-γ stimulation, whereas RUX attenuated their expression in microglia (**Figure 2B**). Moreover, western blotting showed that iNOS ($P = 0.0002$) and COX-2 ($P < 0.0001$) expressions were significantly decreased by treatment with RUX following IFN-γ stimulation (**Figure 2C–E**). Cell proliferation, as measured by the 5-ethynyl-2′-deoxyuridine assay, was clearly decreased after RUX treatment (**Figure 2F**). Consistent with this, expression of Ki67, a cell proliferation marker (Scholzen and Gerdes, 2000), was also inhibited by RUX (**Figure 2G**). Taken together, these results indicate that RUX inhibits IFN-γ–induced microglial inflammation and proliferation.

RUX alleviates inflammation in injured cords after SCI

In vivo, we used the activated microglial marker iNOS to assess microglial-induced neuroinflammation. The distribution of activated p-STAT1+ microglia was then assessed. Immunofluorescence staining showed that the number of $IBA1^+/iNOS^+$ microglia was increased post-SCI; however, administration of RUX reduced this amount (**Figure 3A**). In addition, the increase in the number of $p\text{-}STAT1^+$ microglia was mitigated by treatment with RUX by day 3 post-SCI (**Figure 3A**). We also found that the increased expression of IL-1β, IL-6, TNF-α, and COX-2 post-SCI was significantly reduced by treatment with RUX by day 3 post-SCI (**Figure 3B**). Furthermore, enzyme-linked immunosorbent assays were used to measure the levels of TNF-α, IL-1β, and IL-6 at 1 and 3 days post-SCI. The results showed that high levels of TNF-α, IL-1β, and IL-6 were present at 1 day post-SCI, and that the levels slightly dropped at 3 days post-SCI. Strikingly, mice treated with RUX exhibited a marked decrease in expression of the

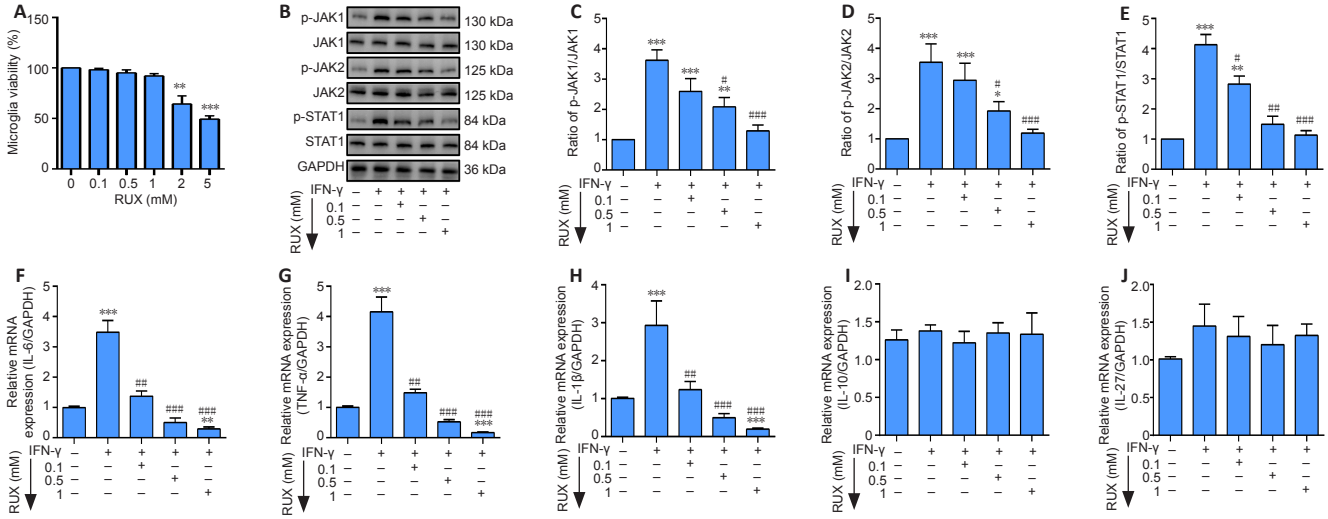

Figure 1 | **RUX mitigates IFN-γ-induced pro-inflammatory cytokines in microglia by targeting the JAK/STAT1 axis.**
Microglia were treated with 0.1, 0.5, or 1 mM RUX for 24 hours, followed by stimulation with IFN-γ (20 ng/mL) for 6 hours. (A) Cell viability of microglia as determined by cell counting kit-8 assay (n = 4 in each group). (B) Western blot of p-JAK1, JAK1, p-JAK2, JAK2, p-STAT1, and STAT1 expression in microglia. (C–E) Quantitation of p-JAK1/JAK1 (C), p-JAK2/JAK2 (D), and p-STAT1/STAT1 (E) ratios in the *in vitro* experiments. (F–J) mRNA expression levels for IL-6 (F), IL-1β (G), TNF-α (H), IL-10 (I), and IL-27 (J) in microglia as determined by quantitative polymerase chain reaction (n = 5 in each group). Data are expressed as mean ± SD. The experiments were repeated four (A) and five (B–J) times; the results shown in C–J were normalized to the Con group. *P < 0.05, **P < 0.01, ***P < 0.001, *vs.* 0 mM/Con group; #P < 0.05, ##P < 0.01, ###P < 0.001, *vs.* IFN-γ group (one-way analysis of variance followed by Tukey's *post hoc* test). GAPDH: Glyceraldehyde-3-phosphate dehydrogenase; IFN-γ: interferon-γ; IL: interleukin; JAK: Janus kinase; p-JAK: phosphorylated Janus kinase; p-STAT1: phosphorylated signal transducer and activator of transcription 1; RUX: ruxolitinib; STAT1: signal transducer and activator of transcription 1; TNF-α: tumor necrosis factor-α.

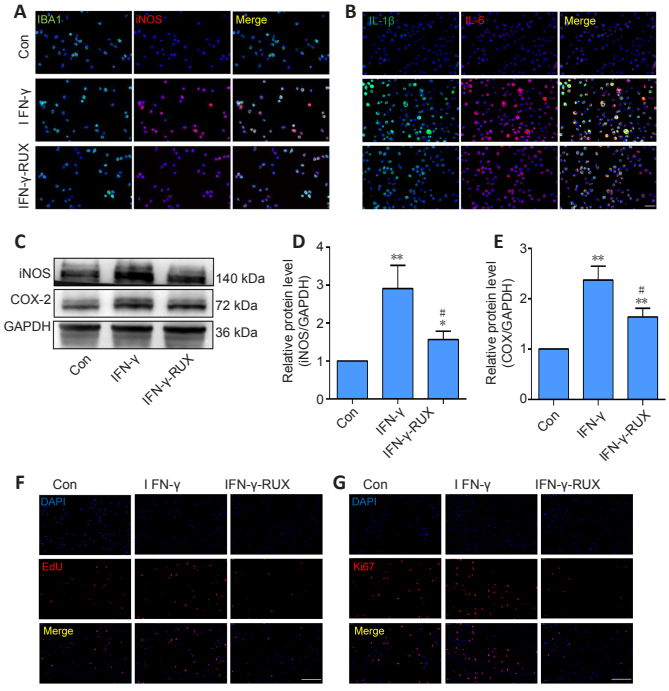

Figure 2 | **RUX reduces microglial activation and proliferation *in vitro*.**
Microglia were treated with 0.1, 0.5, or 1 mM RUX for 24 hours, followed by stimulation with IFN-γ (20 ng/mL) for 6 hours. (A) Representative immunofluorescence images of IBA1$^+$ (green, Alexa Fluor 488)/iNOS$^+$ (red, Alexa Fluor 594) microglia. IFN-γ stimulation increased iNOS expression in microglia, but RUX inhibited this increase. (B) Representative immunofluorescence images of IL-1β$^+$ (green, Alexa Fluor 488) and IL-6$^+$ (red, Alexa Fluor 594) microglia. IFN-γ stimulation increased IL-1β and IL-6 expression in microglia, but RUX reduced this IFN-γ-induced increase. (C) Western blot of iNOS and COX-2 expression in microglia. (D, E) Quantification of iNOS (D) and COX-2 (E) expression. Data are expressed as mean ± SD. The experiments were repeated five times. *P < 0.01, **P < 0.01, *vs.* Con group; #P < 0.05, *vs.* IFN-γ group (one-way analysis of variance followed by Tukey's *post hoc* test). (F) Representative EdU (red) images of microglia. IFN-γ stimulation increased microglia proliferation, but RUX restrained the IFN-γ-induced proliferation. (G) Representative immunofluorescence images of Ki67 (red, Alexa Fluor 594) expression in microglia. IFN-γ stimulation increased the expression of proliferation marker Ki67, but RUX inhibited its expression. Scale bars: 50 μm in A and B; 100 μm in F and G. COX-2: Cyclooxyganese-2; EdU: 5-ethynyl-2′-deoxyuridine; GAPDH: glyceraldehyde-3-phosphate dehydrogenase; IBA1: ionized calcium binding adaptor 1; IFN-γ: interferon-γ; IL: interleukin; iNOS: inducible nitric oxide synthase; RUX: ruxolitinib.

three cytokines compared with the untreated SCI mice on days 1 and 3 post-SCI (P < 0.0001; **Figure 3C** and **D**). H&E staining indicated a smaller area of pathological damage in SCI mice after RUX treatment on day 3 post-SCI (P < 0.0001; **Figure 3E** and **F**). Collectively, these results indicate that RUX reduces the inflammatory response post-SCI.

RUX ameliorates inflammation-induced neuropathology post-SCI

The glial scar, which is composed of microglia and astrocytes, was detected by immunofluorescence staining. At 7 days post-SCI, the initial glial scar had formed; however, the number of microglia and astrocytes was reduced markedly after RUX treatment in SCI mice (P < 0.0001; **Figure 4A–C**). Notably, SCI mice exhibited dispersed distribution of activated microglia; however, we found that activated microglia (indicated with white arrows) gathered near the injured foci, and that other microglia (indicated with yellow arrows) remained distal to the foci (**Figure 4A**). SCI mice treated with RUX consistently showed a less dispersed and smaller glial scar at 28 days post-SCI compared with SCI mice (P < 0.0001; **Figure 4D–F**). Interestingly, RUX administration promoted a reduction in the area of the glial scar, to a point where it encompassed only the injured epicenter, potentially providing more space for axonal regeneration (**Figure 4D**). As expected, severe demyelination and axonal loss were evident at 7 days post-SCI and were significantly ameliorated after RUX treatment (**Figure 4G–I**). Therefore, RUX may protect against secondary neurological injury due to its potent anti-inflammatory properties.

RUX relieves histological and functional disorder following SCI

Given that formation of the glial scar was nearly complete at 28 days post-SCI, we compared histological staining of the injured spinal cord at 7 and 28 days post-SCI. H&E and Nissl staining at 7 days post-SCI showed that treatment with RUX resulted in a larger number of viable neurons compared with untreated mice (P < 0.0001; **Figure 5A–C**) and a reduction in SCI-induced tissue loss. In contrast, the number of neurons was unchanged both in RUX-treated and untreated mice at 28 days post-SCI (P < 0.0001; **Figure 5D–F**). In the swimming test, RUX-treated mice exhibited a smaller angle between their trunk and the water surface, as well as a higher frequency of hindlimb movements compared with SCI mice at 28 days post-SCI (**Figure 5G**). The LSS scores in the SCI + RUX group were higher than those in the SCI group beginning at 14 days post-SCI (P = 0.0109; **Figure 5H**). The Basso mouse scale tests also showed that RUX administration significantly improved locomotor scores beginning at 7 days post-SCI (P < 0.0001; **Figure 5I**). Taken together, these results indicate that treatment with RUX improves tissue protection and functional recovery post-SCI.

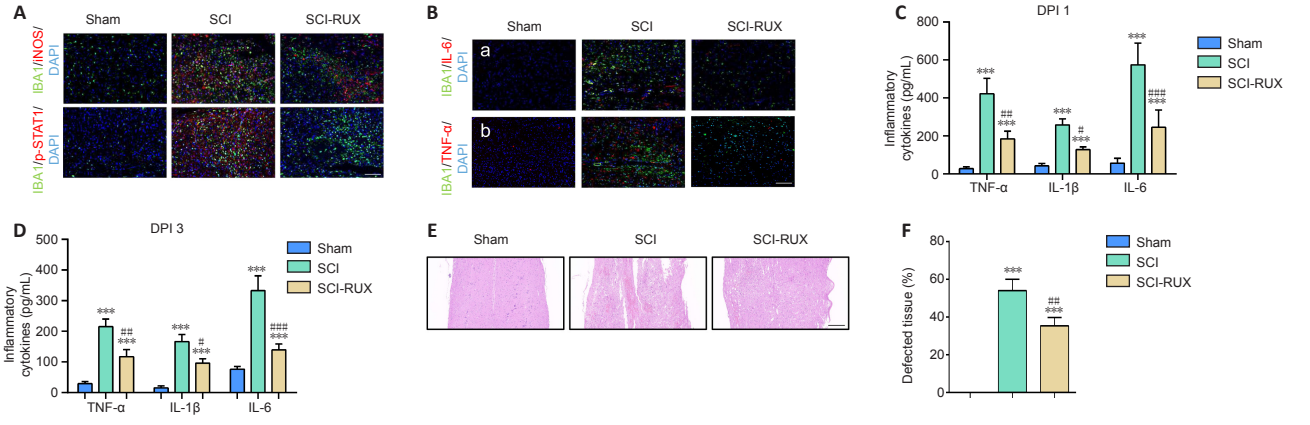

Figure 3 | **RUX alleviates inflammation in the spinal cords of SCI mice.**
(A) Representative immunofluorescence images of IBA1$^+$ (green, Alexa Fluor 488)/iNOS$^+$ (red, Alexa Fluor 594) and IBA$^+$ (green, Alexa Fluor 488)/p-STAT1$^+$ (red, Alexa Fluor 594) microglia in the injured spinal cord at 3 days post-SCI (DPI) in RUX-treated or untreated mice. SCI caused an increase in IBA1$^+$ microglia and promoted the expression of iNOS and p-STAT1 in microglia compared with the sham group, while treatment with RUX reduced the number of IBA1$^+$/iNOS$^+$/p-STAT1$^+$ microglia. (B) Representative immunofluorescence images of IL-1β$^+$ (green, Alexa Fluor 488)/IL-6$^+$ (red, Alexa Fluor 594) and COX-2$^+$ (green, Alexa Fluor 488)/TNF-α$^+$ (red, Alexa Fluor 594) microglia in the injured cord at 3 days post-SCI. SCI led to an increase in the numbers of IL-1β$^+$/IL-6$^+$ and COX-2$^+$/TNF-α$^+$ microglia in the injured spinal cord, but RUX-SCI mice exhibited lower expression of these inflammatory mediators after SCI compared with the SCI mice. (C) TNF-α IL-1β, and IL-6 expression levels as measured by enzyme-linked immunosorbent assay in the injured cord at 1 (C) and 3 (D) days post-SCI. (E) Representative hematoxylin-eosin staining of the injured spinal cord on day 3 post-SCI. SCI caused severe destruction of the spinal cord, but treatment with RUX mitigated the damaged area compared with that seen in the SCI mice. Scale bars: 100 μm in A and B, 200 μm in E. (F) Quantification of tissue integrity in the injured spinal cord (n = 5 per group). Data are expressed as mean ± SD (n = 6 (A–D)/5 (E, F) per group). ***P < 0.001, *vs*. sham group; #P < 0.05, ##P < 0.01, ###P < 0.001, *vs*. SCI group (one-way analysis of variance followed by Tukey's *post hoc* test). COX-2: Cyclooxyganese-2; IBA1: ionized calcium binding adaptor 1; IL: interleukin; iNOS: inducible nitric oxide synthase; p-STAT1: phosphorylated signal transducer and activator of transcription 1; RUX: ruxolitinib; SCI: spinal cord injury; TNF-α: tumor necrosis factor-α.

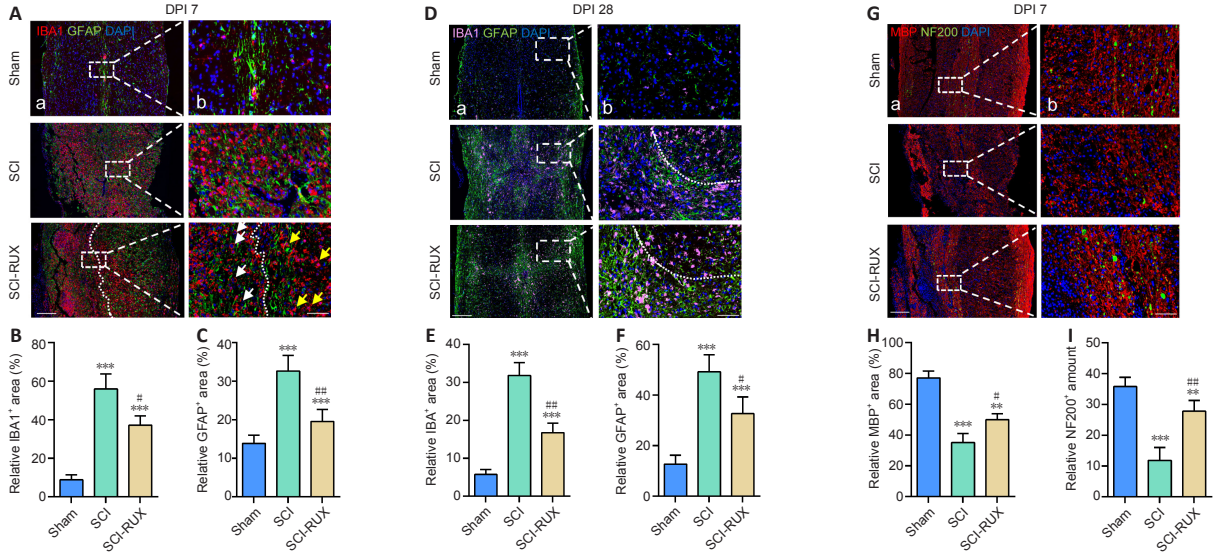

Figure 4 | **RUX ameliorates inflammation-induced neuropathology in SCI mice.**
(A) Representative immunofluorescence images of IBA1$^+$ (red, Alexa Fluor 594)/GFAP$^+$ (green, Alexa Fluor 488) cells in the injured spinal cord at 7 days post-SCI (DPI). The white arrows indicate activated microglia, which have an amoeba-like shape; the yellow arrows indicate the resting branching microglia. The white dashed line separates the relatively proximal and distal injury foci. SCI caused widespread and scattered microglial activation and astrocyte assembly, but treatment with RUX confined the activated microglia to a region proximal to the lesion and reduced the accumulation of astrocytes. (B, C) Quantification of microglia (B) and astrocytes (C) at 7 days post-SCI. (D) Representative immunofluorescence images of IBA1$^+$ (pink, Alexa Fluor 647)/GFAP$^+$ (green, Alexa Fluor 488) cells in the injured spinal cord at day 28 post-SCI. The white dashed line separates tight and loose areas of the glial scar: the area below the line was proximal to lesion, and the area above the line was distal to the lesion. SCI caused widespread and scattered glial scar, but treatment with RUX compacted the glial scar structure closer toward the injury focus. (E, F) Quantification of microglia (E) and astrocytes (F) at 28 days post-SCI. (G) Representative immunofluorescence images of NF200$^+$ (green, Alexa Fluor 488)/MBP$^+$ (red, Alexa Fluor 594) cells in the injured spinal cord at 7 days post-SCI. SCI caused excess loss of myelin and neurofilaments compared with the sham mice, but treatment with RUX partly protected against these effects compared with the SCI mice. Scale bars: 200 μm in A, and 50 μm in B. (H, I) Quantification of myelin (H) and axons (I) in the injured spinal cord at 7 days post-SCI. Data are expressed as mean ± SD (n = 5 per group). **P < 0.01, ***P < 0.001, *vs*. sham group; #P < 0.05, ##P < 0.01, *vs*. SCI group (one-way analysis of variance followed by Tukey's *post hoc* test). GFAP: Glial fibrillary acidic protein; IBA1: ionized calcium binding adaptor 1; MBP: myelin basic protein; NF200: neurofilament 200; RUX: ruxolitinib; SCI: spinal cord injury.

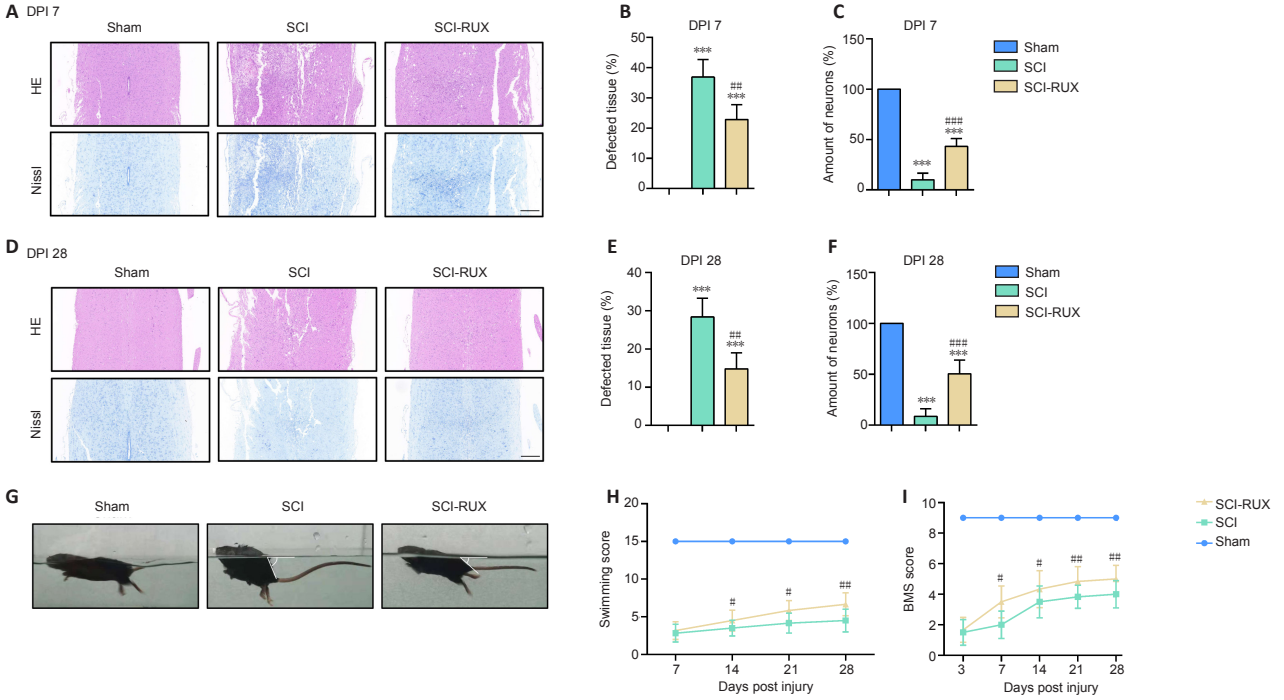

Figure 5 | **RUX reduces the degree of histological damage and functional disorder following SCI.**
(A) Representative HE and Nissl staining of the injured spinal cord at 7 days post-SCI (DPI). Treatment with RUX led to the presence of more complete tissue and more surviving neurons in the injured spinal cords of the SCI-RUX mice compared with those of the SCI mice. (B, C) Quantification of tissue (B) and neuronal (C) integrity in the injured spinal cord at 7 days post-SCI. (D) Representative HE and Nissl staining of the injured spinal cord at 28 days post-SCI. SCI-RUX mice showed superior neurological recovery compared with the SCI mice at 28 days post-SCI. Scale bars: 200 μm. (E, F) Quantification of tissue (E) and neuronal (F) integrity within the injured spinal cord at 28 days post-SCI. (G) Representative photos of mice from the sham, SCI, and SCI-RUX groups swimming at 28 days post-SCI. The white angles indicate the degree of inclination between the water surface and the mouse's trunk. The SCI-RUX mice showed a smaller angle of inclination than the SCI mice while swimming. (H) LSS scores at 7, 14, 21, and 28 days post-SCI. (I) BMS scores at 3, 7, 14, 21, and 28 days post-SCI. High scores indicate good motor function, while low scores indicate poor functional recovery. Data are expressed as mean ± SD (n = 5 (B, C, E, and F)/6 (H, I) in each group). ***P < 0.001, *vs*. sham group; #P < 0.05, ##P < 0.01, ###P < 0.001, *vs.* SCI group (one-way analysis of variance for B, C, E, and F, two-way analysis of variance for H and I, all followed by Tukey's *post hoc* test). BMS: Basso mouse scale; HE: hematoxylin-eosin; LSS: Louisville Swim Scale; RUX: ruxolitinib; SCI: spinal cord injury.

Discussion

In the present study, RUX showed a neuroprotective role in SCI-induced neuropathology by negatively regulating neuroinflammatory levels through targeting the JAK/STAT signaling pathway. RUX inhibited IFN-γ-stimulated inflammation and cell proliferation in cultured microglia *in vitro*, which resulted from the specific inhibition of JAK1/2. As a classic immunomodulatory factor, IFN-γ regulates immunogenesis in various cells, including T-cells, macrophages, and microglia. Increased expression of IFN-γ has been demonstrated to exert an undesirable effect in multiple sclerosis and experimental autoimmune encephalomyelitis (Saraswat et al., 2021; Wang et al., 2021). Strikingly, IFN-γ causes prolonged inflammation following SCI, leading to ongoing damage in a rat model (Kwiecien et al., 2020). Hence, blocking and/or down-regulating the expression of IFN-γ may attenuate the neuroinflammatory response post-SCI. A previous study reported that SOCS3 suppressed the GM-CSF/IFN-γ-induced inflammatory response by inhibiting the activities of JAK1 and JAK2 (Zhang et al., 2020). JAKs, which are activated by cytokines and growth factors, further phosphorylate transcription factor STATs, contributing to the transcription of genes that encode factors that initiate inflammatory responses (Howell et al., 2019). In the current study, RUX, a selective and equipotent JAK1/2 inhibitor, attenuated the IFN-γ-stimulated inflammatory response in microglia in a concentration-dependent manner. Prolonged hyperinflammation not only produces redundant pro-inflammatory mediators that aggravate tissue degradation but also leads to excessive microglial pyroptosis, both of which exacerbate necrosis (Liu et al., 2018; Tsuchiya et al., 2019). Importantly, RUX was shown to ameliorate the "cytokine storm" in a hemophagocytic lymphohistiocytosis mouse model of hyperinflammation syndrome (Huarte et al., 2021). Although high RUX concentrations resulted in decreased cell viability, an appropriate concentration range resulted in significantly decreased expression of the pro-inflammatory cytokines IL-1β, IL-6, and TNF-α. Furthermore, RUX decreased the expression of iNOS and COX-2, indicating that RUX largely inhibited the transition from resting microglia to activated, pro-inflammatory microglia, which decreased neuroinflammation.

Microglial proliferation is another important aspect of neurological remodeling. Excessive proliferation and recruitment of microglia have been implicated in an increase in the glial scar (Todd et al., 2019), which impedes axonal regeneration (Orr and Gensel, 2018) and accelerates widespread histolysis by inflammatory microglia–secreted matrix metalloproteinases (Jiang et al., 2021). Inhibition of JAKs has been reported to induce compromised cell proliferation and invasion by arresting the cell cycle in tumor cells (Lu et al., 2017; Gao et al., 2020; She et al., 2020). Interestingly, we found that RUX decreased microglial proliferation after IFN-γ stimulation. We also found that microglial proliferation was reduced following RUX.

The activation of pro-inflammatory microglia that express iNOS and COX2 in the early stage of SCI plays a crucial role in neuroinflammation, and at the same time their morphology changes from a ramified shape to an amoeboid shape (Manivannan et al., 2013; Nguyen et al., 2020; Yao et al., 2020). Therefore, the presence of more amoeba-like microglia indicates more severe secondary damage and more intense neuroinflammation in the injured spinal cord after SCI. In our *in vivo* studies, we found that pro-inflammatory microglia with amoeboid-like morphologies were highly concentrated in the immediate vicinity of the injured foci, and that the number of microglia was proportional to the distance from the injury foci in RUX-treated mice. In contrast, extensive populations of microglia with amoeboid-like morphologies were observed in SCI mice at 7 days post-SCI, suggesting that inflammation was widespread in the injured spinal cords and likely caused increased pathology and neuronal loss. However, administration of RUX ameliorated the extent of the lesion. Indeed, at 28 days post-SCI RUX not only markedly reduced the area of the glial scar but also largely accelerated the progression of scar healing. In the acute inflammatory phase, activated microglia and infiltrating macrophages that contact axons can cause axonal retraction, resulting in long-distance axons withdrawing from their original location (Busch et al., 2009; Evans et al., 2014). Unfortunately, spontaneous axonal regeneration in the post-inflammatory phase is rare because of the inflammatory-driven glial scar. However, centripetal migration of activated microglia has been shown to result in spontaneous healing after SCI (Kobayakawa et al., 2019; Deng et

al., 2021), which also reduces axonal retraction and neuronal death. In addition, activated microglia directly induce oligodendrocyte apoptosis and cause demyelination. Here, RUX administration was shown not only to protect axons and myelin structure but also to promote centripetal migration of inflammatory microglia to the injured foci, suggesting that RUX may have a potent neuroprotective effect in addition to its anti-inflammatory activities. Taken together, our results show that RUX attenuates inflammatory responses and microglial proliferation by inhibiting IFN-γ-mediated stimulation of the JAK/STAT signaling pathway. Administration of RUX to SCI mice reduced the size of the glial scar, protected neurons and axons, and improved hindlimb locomotor recovery by inhibiting inflammation and promoting centripetal migration of microglia. This preliminary study focused on the exact pharmacological activity of RUX in the context of post-SCI inflammation and neuropathy; however, future studies are needed to determine the precise RUX dosage required and its potential side effects. A comprehensive evaluation of RUX may reveal its potential value in immunotherapy for SCI.

This study had several limitations. First, we focused on only part of the pathology of SCI and demonstrated the importance of the anti-inflammatory activity of RUX, but its effects on other important consequences of SCI were not investigated. Second, the effects of RUX in other neural cells like neurons, astrocytes and oligodendrocytes were not investigated. Thus, our further researches are needed to systematacially trace the role of RUX in neurological pathophysiology post SCI.

In summary, RUX attenuates inflammatory responses and cell proliferation by selectively inhibiting the JAK/STAT signaling pathway in IFN-γ-stimulated microglia, leading to inhibition of glial scar formation, decreased demyelination, and reduced axonal retraction and neuronal cell death.

Acknowledgments: *We thank for the technology support from the Central Lab of Taizhou People's Hospital, China.*
Author contributions: *Study conception and design: XJC, HJL; animal model establishment: ZYH, AD; experiment implementation: ZYQ, RYK, SZ, BYW, JChang; data analysis: JCao, CQW; manuscript draft: LY; study supervision: XJC, LY, HJL. All authors approved the final version of the manuscript.*
Conflicts of interest: *The authors have no conflict of interest.*

References

Aguzzi A, Barres BA, Bennett ML (2013) Microglia: scapegoat, saboteur, or something else? Science 339:156-161.
Ahuja CS, Wilson JR, Nori S, Kotter MRN, Druschel C, Curt A, Fehlings MG (2017) Traumatic spinal cord injury. Nat Rev Dis Primers 3:17018.
Ajayi S, Becker H, Reinhardt H, Engelhardt M, Zeiser R, von Bubnoff N, Wäsch R (2018) Ruxolitinib. Recent Results Cancer Res 212:119-132.
Busch SA, Horn KP, Silver DJ, Silver J (2009) Overcoming macrophage-mediated axonal dieback following CNS injury. J Neurosci 29:9967-9976.
Cao Y, Wei J, Zou L, Jiang T, Wang G, Chen L, Huang L, Meng F, Huang L, Wang N, Zhou X, Luo H, Mao Z, Chen X, Xie J, Liu J, Cheng H, Zhao J, Huang G, Wang W, et al. (2020) Ruxolitinib in treatment of severe coronavirus disease 2019 (COVID-19): A multicenter, single-blind, randomized controlled trial. J Allergy Clin Immunol 146:137-146.e3.
Das R, Guan P, Sprague L, Verbist K, Tedrick P, An QA, Cheng C, Kurachi M, Levine R, Wherry EJ, Canna SW, Behrens EM, Nichols KE (2016) Janus kinase inhibition lessens inflammation and ameliorates disease in murine models of hemophagocytic lymphohistiocytosis. Blood 127:1666-1675.
David S, Kroner A (2011) Repertoire of microglial and macrophage responses after spinal cord injury. Nat Rev Neurosci 12:388-399.
Delen E, Doğanlar O (2020) The dose dependent effects of ruxolitinib on the invasion and tumorigenesis in gliomas cells via inhibition of interferon gamma-depended JAK/STAT signaling pathway. J Korean Neurosurg Soc 63:444-454.
Deng LX, Liu NK, Wen RN, Yang SN, Wen X, Xu XM (2021) Laminin-coated multifilament entubulation, combined with Schwann cells and glial cell line-derived neurotrophic factor, promotes unidirectional axonal regeneration in a rat model of thoracic spinal cord hemisection. Neural Regen Res 16:186-191.
Evans TA, Barkauskas DS, Myers JT, Hare EG, You JQ, Ransohoff RM, Huang AY, Silver J (2014) High-resolution intravital imaging reveals that blood-derived macrophages but not resident microglia facilitate secondary axonal dieback in traumatic spinal cord injury. Exp Neurol 254:109-120.
Gao J, Xia R, Chen J, Gao J, Luo X, Ke C, Ren C, Li J, Mi Y (2020) Inhibition of esophageal-carcinoma cell proliferation by genistein via suppression of JAK1/2-STAT3 and AKT/MDM2/p53 signaling pathways. Aging (Albany NY) 12:6240-6259.
Gottfried-Blackmore A, Kaunzner UW, Idoyaga J, Felger JC, McEwen BS, Bulloch K (2009) Acute in vivo exposure to interferon-gamma enables resident brain dendritic cells to become effective antigen presenting cells. Proc Natl Acad Sci U S A 106:20918-20923.
Hong X, Jiang F, Li Y, Fang L, Qian Z, Chen H, Kong R (2020) Treatment with 5-methoxytryptophan attenuates microglia-induced neuroinflammation in spinal cord trauma. Int Immunopharmacol 88:106988.
Howell MD, Kuo FI, Smith PA (2019) Targeting the janus kinase family in autoimmune skin diseases. Front Immunol 10:2342.
Huarte E, Peel MT, Verbist K, Fay BL, Bassett R, Albeituni S, Nichols KE, Smith PA (2021) Ruxolitinib, a JAK1/2 inhibitor, ameliorates cytokine storm in experimental models of hyperinflammation syndrome. Front Pharmacol 12:650295.
Huo M, Cao X, Zhang H, Lau CW, Hong H, Chen FM, Huang Y, Chawla A, Tian XY (2021) Loss of myeloid Bmal1 exacerbates hypertensive vascular remodelling through interaction with STAT6 in mice. Cardiovasc Res doi: 10.1093/cvr/cvab336.
Jiang S, Wu Y, Wu S, Ye S, Kong R, Chang J, Xia M, Bao J, Peng X, Hong X, Qian Z, Li H (2021) Silencing TAK1 reduces MAPKs-MMP2/9 expression to reduce inflammation-driven neurohistological disruption post spinal cord injury. Cell Death Discov 7:96.
Kelchtermans H, Billiau A, Matthys P (2008) How interferon-gamma keeps autoimmune diseases in check. Trends Immunol 29:479-486.
Kobayakawa K, Ohkawa Y, Yoshizaki S, Tamaru T, Saito T, Kijima K, Yokota K, Hara M, Kubota K, Matsumoto Y, Harimaya K, Ozato K, Masuda T, Tsuda M, Tamura T, Inoue K, Edgerton VR, Iwamoto Y, Nakashima Y, Okada S (2019) Macrophage centripetal migration drives spontaneous healing process after spinal cord injury. Sci Adv 5:eaav5086.
Kong FQ, Zhao SJ, Sun P, Liu H, Jie J, Xu T, Xu AD, Yang YQ, Zhu Y, Chen J, Zhou Z, Qian DF, Gu CJ, Chen Q, Yin GY, Zhang HW, Fan J (2020) Macrophage MSR1 promotes the formation of foamy macrophage and neuronal apoptosis after spinal cord injury. J Neuroinflammation 17:62.
Kroner A, Rosas Almanza J (2019) Role of microglia in spinal cord injury. Neurosci Lett 709:134370.
Kwiecien JM, Dabrowski W, Dąbrowska-Bouta B, Sulkowski G, Oakden W, Kwiecien-Delaney CJ, Yaron JR, Zhang L, Schutz L, Marzec-Kotarska B, Stanisz GJ, Karis JP, Struzynska L, Lucas AR (2020) Prolonged inflammation leads to ongoing damage after spinal cord injury. PLoS One 15:e0226584.
Li Y, Ritzel RM, Khan N, Cao T, He J, Lei Z, Matyas JJ, Sabirzhanov B, Liu S, Li H, Stoica BA, Loane DJ, Faden AI, Wu J (2020) Delayed microglial depletion after spinal cord injury reduces chronic inflammation and neurodegeneration in the brain and improves neurological recovery in male mice. Theranostics 10:11376-11403.
Liang WC, Ren JL, Yu QX, Li J, Ng TK, Chu WK, Qin YJ, Chu KO, Schally AV, Pang CP, Chan SO (2020) Signaling mechanisms of growth hormone-releasing hormone receptor in LPS-induced acute ocular inflammation. Proc Natl Acad Sci U S A 117:6067-6074.
Liu W, Chen Y, Meng J, Wu M, Bi F, Chang C, Li H, Zhang L (2018) Ablation of caspase-1 protects against TBI-induced pyroptosis in vitro and in vivo. J Neuroinflammation 15:48.
Livak KJ, Schmittgen TD (2001) Analysis of relative gene expression data using real-time quantitative PCR and the 2(-Delta Delta C(T)) Method. Methods 25:402-408.
Lu Z, Hong CC, Jark PC, Assumpção A, Bollig N, Kong G, Pan X (2017) JAK1/2 Inhibitors AZD1480 and CYT387 Inhibit Canine B-Cell Lymphoma Growth by Increasing Apoptosis and Disrupting Cell Proliferation. J Vet Intern Med 31:1804-1815.
Madore C, Yin Z, Leibowitz J, Butovsky O (2020) Microglia, lifestyle stress, and neurodegeneration. Immunity 52:222-240.
Manivannan J, Tay SS, Ling EA, Dheen ST (2013) Dihydropyrimidinase-like 3 regulates the inflammatory response of activated microglia. Neuroscience 253:40-54.
Nguyen LH, Ong W, Wang K, Wang M, Nizetic D, Chew SY (2020) Effects of miR-219/miR-338 on microglia and astrocyte behaviors and astrocyte-oligodendrocyte precursor cell interactions. Neural Regen Res 15:739-747.
Orr MB, Gensel JC (2018) Spinal cord injury scarring and inflammation: therapies targeting glial and inflammatory responses. Neurotherapeutics 15:541-553.
Overstreet AM, LaTorre DL, Abernathy-Close L, Murphy SF, Rhee L, Boger AM, Adlaka KR, Iverson AM, Bakke DS, Weber CR, Boone DL (2018) The JAK inhibitor ruxolitinib reduces inflammation in an ILC3-independent model of innate immune colitis. Mucosal Immunol 11:1454-1465.
Papageorgiou IE, Lewen A, Galow LV, Cesetti T, Scheffel J, Regen T, Hanisch UK, Kann O (2016) TLR4-activated microglia require IFN-γ to induce severe neuronal dysfunction and death in situ. Proc Natl Acad Sci U S A 113:212-217.
Percie du Sert N, Ahluwalia A, Alam S, Avey MT, Baker M, Browne WJ, Clark A, Cuthill IC, Dirnagl U, Emerson M, Garner P, Holgate ST, Howells DW, Hurst V, Karp NA, Lazic SE, Lidster K, MacCallum CJ, Macleod M, Pearl EJ, et al. (2020) Reporting animal research: Explanation and elaboration for the ARRIVE guidelines 2.0. PLoS Biol 18:e3000411.
Pouly S, Becher B, Blain M, Antel JP (2000) Interferon-gamma modulates human oligodendrocyte susceptibility to Fas-mediated apoptosis. J Neuropathol Exp Neurol 59:280-286.
Ren H, Chen X, Tian M, Zhou J, Ouyang H, Zhang Z (2018) Regulation of inflammatory cytokines for spinal cord injury repair through local delivery of therapeutic agents. Adv Sci (Weinh) 5:1800529.
Saijo K, Glass CK (2011) Microglial cell origin and phenotypes in health and disease. Nat Rev Immunol 11:775-787.
Saraswat D, Welliver RR, Ravichandar R, Tripathi A, Polanco JJ, Broome J, Hurley E, Dutta R, Feltri ML, Sim FJ (2021) Heparanome-mediated rescue of oligodendrocyte progenitor quiescence following inflammatory demyelination. J Neurosci 41:2245-2263.
Schneider CA, Rasband WS, Eliceiri KW (2012) NIH Image to ImageJ: 25 years of image analysis. Nat Methods 9:671-675.
Scholzen T, Gerdes J (2000) The Ki-67 protein: from the known and the unknown. J Cell Physiol 182:311-322.
She S, Zhao Y, Kang B, Chen C, Chen X, Zhang X, Chen W, Dan S, Wang H, Wang YJ, Zhao J (2020) Combined inhibition of JAK1/2 and DNMT1 by newly identified small-molecule compounds synergistically suppresses the survival and proliferation of cervical cancer cells. Cell Death Dis 11:724.
Silva NA, Sousa N, Reis RL, Salgado AJ (2014) From basics to clinical: a comprehensive review on spinal cord injury. Prog Neurobiol 114:25-57.
Todd L, Palazzo I, Suarez L, Liu X, Volkov L, Hoang TV, Campbell WA, Blackshaw S, Quan N, Fischer AJ (2019) Reactive microglia and IL1β/IL-1R1-signaling mediate neuroprotection in excitotoxin-damaged mouse retina. J Neuroinflammation 16:118.
Too LK, Mitchell A (2021) Brains, bacteria and behaviors: the role of interferon-gamma in the pathogenesis of pneumococcal meningitis. Neural Regen Res 16:125-126.
Tsuchiya K, Nakajima S, Hosojima S, Thi Nguyen D, Hattori T, Manh Le T, Hori O, Mahib MR, Yamaguchi Y, Miura M, Kinoshita T, Kushiyama H, Sakurai M, Shiroishi T, Suda T (2019) Caspase-1 initiates apoptosis in the absence of gasdermin D. Nat Commun 10:2091.
Walker JM (1994) The bicinchoninic acid (BCA) assay for protein quantitation. Methods Mol Biol 32:5-8.
Wang X, Li B, Liu L, Zhang L, Ma T, Guo L (2021) Nicotinamide adenine dinucleotide treatment alleviates the symptoms of experimental autoimmune encephalomyelitis by activating autophagy and inhibiting the NLRP3 inflammasome. Int Immunopharmacol 90:107092.
Yan B, Freiwald T, Chauss D, Wang L, West E, Mirabelli C, Zhang CJ, Nichols EM, Malik N, Gregory R, Bantscheff M, Ghidelli-Disse S, Kolev M, Frum T, Spence JR, Sexton JZ, Alysandratos KD, Kotton DN, Pittaluga S, Bibby J, et al. (2021) SARS-CoV-2 drives JAK1/2-dependent local complement hyperactivation. Science immunology 6:eabg0833.
Yao Z, Liu N, Zhu X, Wang L, Zhao Y, Liu Q, Gao C, Li J (2020) Subanesthetic isoflurane abates ROS-activated MAPK/NF-κB signaling to repress ischemia-induced microglia inflammation and brain injury. Aging (Albany NY) 12:26121-26139.
Zhang X, He B, Li H, Wang Y, Zhou Y, Wang W, Song T, Du N, Gu X, Luo Y, Wang Y (2020) SOCS3 attenuates GM-CSF/IFN-γ-mediated inflammation during spontaneous spinal cord regeneration. Neurosci Bull 36:778-792.
Zhou T, Zheng Y, Sun L, Badea SR, Jin Y, Liu Y, Rolfe AJ, Sun H, Wang X, Cheng Z, Huang Z, Zhao N, Sun X, Li J, Fan J, Lee C, Megraw TL, Wu W, Wang G, Ren Y (2019) Microvascular endothelial cells engulf myelin debris and promote macrophage recruitment and fibrosis after neural injury. Nat Neurosci 22:421-435.

C-Editor: Zhao M; S-Editors: Yu J, Li CH; L-Editors: Crow E, Yu J, Song LP; T-Editor: Jia Y